THE ASTROPHYSICAL JOURNAL, 364:15–22, 1990 November 20

NEW OBSERVATIONS[1] AND GRAVITATIONAL LENS MODELS OF THE CLOVERLEAF QUASAR H1413+117

R. KAYSER,[2] J. SURDEJ,[3,4] J. J. CONDON,[5] K. I. KELLERMANN,[5] P. MAGAIN,[3]
M. REMY,[6] AND A. SMETTE[7]

Received 1989 August 14; accepted 1990 May 22

ABSTRACT

New optical and radio observations of the quadruple quasar H1413+117, the Cloverleaf, carried out with the 1.54 m Danish telescope at ESO and with the VLA at NRAO are presented. The VLA data, obtained in the A configuration at 3.6 cm, show radio counterparts at the positions of the four optical images and an additional strong radio source between images B and D. Gravitational lens models of H1413+117 using (*a*) a single elliptical galaxy and (*b*) two spherical galaxies are presented, which fit the positions of the four images of the quasar remarkably well. The models suggest that the strong radio source is a feature of the quasar, e.g., an ejected blob, which lies right on the caustic of the lens and is thereby strongly amplified. The time delays predicted by our models are sufficiently short to allow for their determination within one observational season, making H1413+117 an exceptionally well suited object for gravitational lens research.

Subject headings: gravitational lenses — quasars

I. INTRODUCTION

The discovery of the first gravitationally lensed quasar 0957+561 (Walsh, Carswell, and Weymann 1979), more than 40 years after Zwicky's (1937*a*, *b*) proposal that multiple images of distant objects lensed by foreground galaxies should be detectable, led to an outburst of theoretical as well as observational work on gravitational lensing (for recent reviews see, e.g., Blandford and Kochanek 1987; Nottale 1988; Refsdal and Kayser 1988; Turner 1989; Hewitt 1989; Surdej 1990). Lensed quasars and galaxies (giant arcs) obviously probe the distribution of luminous and dark matter in the universe and can be used to determine independently the masses of galaxies and clusters of galaxies (Refsdal 1964; Borgeest 1986). The time delay between the images of a lensed quasar (or between the images of a supernova in lensed galaxies) may be used to determine the Hubble parameter without climbing up the cosmological distance ladder (Refsdal 1964; Kayser and Refsdal 1983; Kayser 1986; Gorenstein, Falco, and Shapiro 1988). Gravitational microlensing may offer a possibility to learn about the size and the structure of the energy source of active galactic nuclei, as well as about the mass spectrum of compact objects in the lensing galaxy (Gott 1981; Canizares 1981, 1982; Grieger, Kayser and Refsdal 1988).

Another very important aspect of gravitational lensing is the *amplification bias*: lensing may influence the quasar luminosity function (see, e.g., Turner 1988 for a review) (*a*) globally, thereby mimicking evolution, and (*b*) locally near foreground galaxies, thereby producing apparent quasar-galaxy associations (Webster *et al.* 1988; Schneider 1988; and references therein).

To better understand the quasar luminosity function (and thereby, we hope, the quasar phenomenon itself), we obviously need to understand the influence of lensing on it, thus the statistical evaluation of gravitational lensing within well-defined samples of quasars is of great importance. Several surveys for lensed objects are under way (Hewitt *et al.* 1989; Surdej *et al.* 1988*b*; Wester, Hewett, and Irwin 1988; Crampton *et al.* 1989), using different selection criteria and methods, in order to perform this ambitious task.

In 1986 November, we began an optical survey for lensed objects among the apparently ($m_v < 17.5$) and intrinsically ($M_v < -29.0$) highly luminous quasars (hereafter HLQs). These objects form a particularly promising sample since (*a*), the probability of lensing is higher in a flux-limited sample than in a volume-limited one (Turner, Ostriker, and Gott 1984), (*b*) the HLQs are the most likely objects for which the "intrinsic" brightness may in part be due to lensing, and (*c*) the large cosmological distances of the HLQs imply a higher probability for galaxies to be located along their lines of sight.

Our project has led to the discovery of two new lens systems, UM 673 = Q0142+100 (Surdej *et al.* 1987; Surdej *et al.* 1988*a*) and H1413+117 (Magain *et al.* 1988) as well as several promising candidates (Surdej *et al.* 1988*b*).

H1413+117 ($z_q = 2.55$, $m_v = 17$) is one of the brightest members of the class of broad absorption line (BAL) quasars. The spectrum of H1413+117 shows two narrow absorption systems at redshifts 1.66 and 2.07 (Hazard *et al.* 1984; Drew and Boksenberg 1984; Turnshek *et al.* 1988). Under good seeing conditions (0".8 FWHM), we have been able to resolve H1413+117 into a cloverleaf with four components having comparable brightness, separated by $\approx 1''$ (Magain *et al.* 1988). We have shown that the spectra observed for two of the four images are identical (apart from sharp absorption line systems at $z = 1.44$ and $z = 1.66$, which are much stronger in component B; Magain *et al.* 1988), and quite similar to that of the whole integrated image, thereby supporting the hypothesis that H1413+117 is one quasar quadruply imaged by a foreground gravitational lens.

In this paper, we present new optical and radio observations of the Cloverleaf H1413+117, as well as gravitational lens

[1] Collected at the European Southern Observatory, La Silla, Chile and at the National Radio Astronomy Observatory, Socorro, New Mexico.

[2] CITA, Toronto, Ontario.
[3] Institut d'Astrophysique, Cointe-Ougrée, Belgium.
[4] Also, Chercheur Qualifié au Fonds National de la Recherche Scientifique (Belgium).
[5] NRAO, Charlottesville, Virginia.
[6] ESO, La Silla, Chile.
[7] ESO, Garching, Federal Republic of Germany.

models accounting for the new observed properties of this exceptional object.

II. NEW OBSERVATIONS

a) Optical

New images of H1413+117 were obtained (by P. M. and M. R.) on 1988 April 27 with the Danish 1.54 m telescope at ESO, La Silla. In particular, *B* and *I* images were obtained under a seeing of 1".0 and 0".8, respectively. The positions and brightness ratios, relative to image A are listed in Table 1. Contamination of the red images by a foreground galaxy may introduce errors in the derived positions and brightness ratios.

In the case of image D, the *R* magnitude obtained on April 27 is found to be significantly fainter than the one which was obtained on April 8 (published in Magain *et al.* 1988). Image D has clearly faded between the two observations.

We have also made use of the average seeing (FWHM = 1".7), 20 minute *R* CCD exposure of H1413+117 obtained (by P. M.) with the ESO/MPI 2.2 m telescope (pixel size = 0".35) on 1987 April 29 in order to detect and catalog all objects located in the vicinity of the Cloverleaf. Taking as a reference the brightest lensed image A, the relative positions, type (star or galaxy), and integrated *R* magnitude of the 59 detected objects are listed in Table 2. The *R* brightness of image A has has been assumed to be 18.30. Without taking into account the error on m_R(A), the m_R are precise at about ± 0.15 mag. Figure 1 illustrates the location of the objects on the CCD frame. The objects have been selected using the following criteria: (1) they are at most 5.75 mag fainter than image A, i.e., 3 σ above the background; (2) the FWHM of a fitted Gaussian profile is at least 1".4 in order to discriminate real objects from cosmic rays and small-scale spatial variations of the sky background. Objects with FWHM greater than 2".1 and at most 5 mag fainter than image A have been listed as galaxies.

b) Radio

Radio observations of the Cloverleaf have been obtained with the Very Large Array (VLA) of the National Radio Astronomy Observatory (NRAO, Socorro, New Mexico) on both 1989 January 13 (J. S. and K. I. K.) and February 4 (J. J. C.), using the A array configuration. During these two independent runs, we observed for 90 minutes at 8.415 GHz (3.6 cm) with a bandwidth of 100 MHz in each of the two circular polarizations. The source 1413+135 at B1950 position $\alpha = 14^h\ 13^m\ 33^s.91$, $\delta = 13°34'17".4$ was observed as a phase calibrator. The two sets were edited and calibrated, and the visibility data were combined, Fourier-transformed with natural weighting, CLEANed, and restored with a 0".3 FWHM Gaussian beam using the AIPS reduction package. The r.m.s. noise on the natural weighted image made from combined data is 0.012 mJy. This image is shown in Figure 2. As can be seen, H1413+117 appears to be fully resolved at radio wavelengths.

TABLE 1

RELATIVE OPTICAL POSITIONS AND BRIGHTNESS RATIOS OF IMAGES B, C, AND D WITH RESPECT TO A

	Δα			Δδ			*r*		
IMAGE	*R*	*I*	*B*	*R*	*I*	*B*	*R*	*I*	*B*
B.....	0".76	0".75	0".78	0".17	0".17	0".16	0".85	0".90	0".84
C.....	−0.51	−0.51	−0.50	0.72	0.73	0.72	0.74	0.76	0.83
D.....	0.38	0.35	0.36	1.07	1.07	1.06	0.61	0.59	0.61

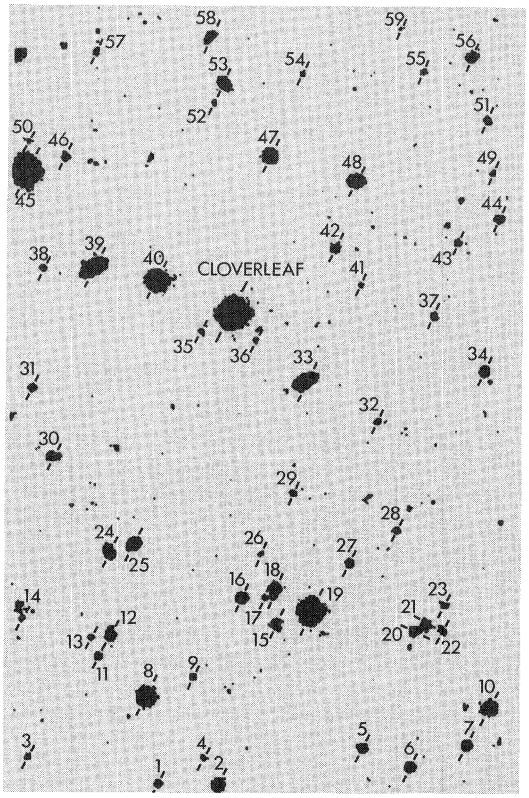

FIG. 1.—Reproduction of the 20 minute *R* CCD frame with each of the 59 objects detected near H1413+117 (see text and Table 2). North is up, and east is to the left; the field size is 2' × 3'. Note that due to less than optimal seeing conditions, the Cloverleaf is not resolved on this frame.

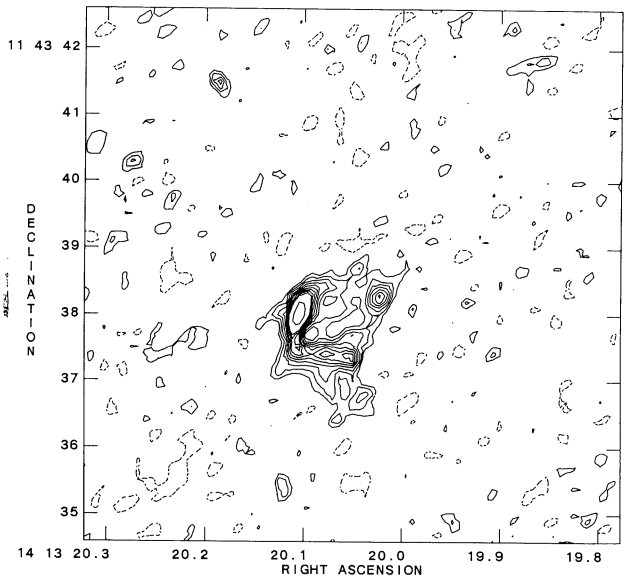

FIG. 2.—VLA map at 8.4 GHz of the field near H1413+117. The beam size is about 0".3 FWHM. The contour levels are at −0.02, 0.02, 0.03, 0.04, 0.05, 0.06, 0.07, 0.08, 0.09, 0.10, 0.15 and 0.20 mJy beam^{-1}. Note that the closed contour centered about 0".5 south and 0".5 east of C corresponds to a local minimum.

TABLE 2

OBJECTS IN THE VICINITY OF THE CLOVERLEAF[a]

Number	Δα	Δδ	m_R	Type	Number	Δα	Δδ	m_R	Type
1.....	16″.71	−105″.95	22.71	Star	31.....	45″.46	−16″.52	22.71	Star
2.....	3.24	−106.22	20.68	Star	32.....	−32.38	−24.24	23.30	Star
3.....	46.07	−99.80	23.35	Star	33.....	−16.47	−15.11	20.47	Galaxy
4.....	6.46	−100.13	23.37	Star	34.....	−56.66	−12.84	22.22	Galaxy
5.....	−29.31	−97.88	22.11	Star	35.....	7.40	−3.87	23.69	Star
6.....	−40.16	−102.34	21.89	Star	36.....	−4.82	−5.82	23.72	Star
7.....	−52.90	−97.52	21.57	Star	37.....	−45.16	−0.62	23.05	Star
8.....	−19.48	−86.28	18.91	Star	38.....	43.21	10.46	23.33	Star
9.....	9.00	−81.76	23.18	Star	39.....	31.80	10.46	19.90	Galaxy
10.....	−57.84	−88.98	21.36	Galaxy	40.....	17.38	7.66	18.39	Star
11.....	30.21	−77.09	22.99	Star	41.....	−28.55	6.60	23.73	Star
12.....	31.88	−72.89	23.63	Star	42.....	−22.70	14.90	22.53	Galaxy
13.....	27.54	−72.61	21.76	Star	43.....	−50.48	16.11	23.31	Star
14.....	47.57	−68.10	23.16	Star	44.....	−59.85	21.55	22.40	Star
15.....	9.63	−69.97	22.33	Galaxy	45.....	47.27	32.45	16.91	Star
16.....	−1.93	−64.07	21.18	Star	46.....	38.18	35.62	22.71	Star
17.....	−7.20	−63.90	23.57	Star	47.....	−7.99	35.68	20.13	Star
18.....	−9.41	−62.08	21.84	Star	48.....	27.28	30.12	20.97	Galaxy
19.....	−17.59	−67.11	17.89	Star	49.....	−58.22	31.79	23.34	Star
20.....	−41.14	−71.54	22.36	Galaxy	50.....	46.56	39.16	23.31	Star
21.....	−43.49	−70.16	22.23	Star	51.....	−56.96	43.68	22.97	Star
22.....	−47.24	−71.41	22.75	Star	52.....	4.90	47.73	23.87	Star
23.....	−47.74	−65.74	23.49	Star	53.....	2.54	52.03	21.35	Galaxy
24.....	28.03	−53.62	21.65	Galaxy	54.....	15.17	54.16	23.51	Star
25.....	22.45	−51.97	21.48	Galaxy	55.....	−42.56	54.76	23.43	Star
26.....	−6.27	−54.15	23.63	Star	56.....	−53.36	57.96	21.97	Star
27.....	−26.30	−56.26	22.55	Star	57.....	38.61	60.54	23.37	Star
28.....	−36.80	−48.81	22.98	Star	58.....	5.76	62.73	22.06	Galaxy
29.....	−13.45	−40.48	23.42	Star	59.....	−37.33	64.44	23.26	Star
30.....	40.69	−32.04	22.00	Galaxy					

[a] See text.

The shape of the radio structure is quite similar to that of the optical Cloverleaf pattern, except for the presence of a relatively bright radio component (peak flux density of 0.195 mJy beam^{-1}) centered near $\alpha = 14^h13^m10^s.1$, $\delta = 11°43'38''$. This mysterious strong radio source will be referred hereafter as to the SRS component. The peak flux densities of the radio components A, B, and C′ are 0.088, 0.171, 0.081 mJy beam^{-1}, respectively.

c) *Comparison of Optical and Radio Data*

In order to best adjust the overlap between the optical and radio images of the Cloverleaf (see Fig. 3), we have first made an attempt to identify the possible radio counterparts of the 59 optically selected objects listed in Table 2. Unfortunately, apart from H1413+117 itself, none of these objects were detected on the VLA image. Since the VLA radio position of the Cloverleaf is accurate to better than 0″.1, the best we could do to match the radio and optical positions consisted in performing accurate astrometric measurements of the integrated image of H1413+117 on the basis of an ESO Schmidt plate kindly taken for us by O. Pizarro. After various careful measurements by one of us (A. S.), the optical centroid of H1413+117 was derived to be $\alpha = 14^h13^m20^s.11 \pm 0^s.04$, $\delta = 11°43'37''.8 \pm 0''.4$ for the 1950.0 equinox, which is in good agreement with the position given by Hazard *et al.* (1984). This measured position actually coincides with the southernmost part of the SRS feature seen on the VLA map (see the large triangle marked in Fig. 3). However, the best visual overlap that we could achieve between the radio and optical images of H1413+117 leads to a very slightly different position for the optical centroid (see Fig. 3). The difference between this and the previous optical position amounts to approximately 0″.6, i.e., only 1.5 times the formal uncertainties of our astrometric measurements. Of course, this match between the optical and radio images of H1413+117 needs to be further checked on the basis of a higher sensitivity map to be obtained with the VLA. Further comparison between the optical and radio data of H1413+117 (see Figs. 2 and 3) indicates that images A, B, and

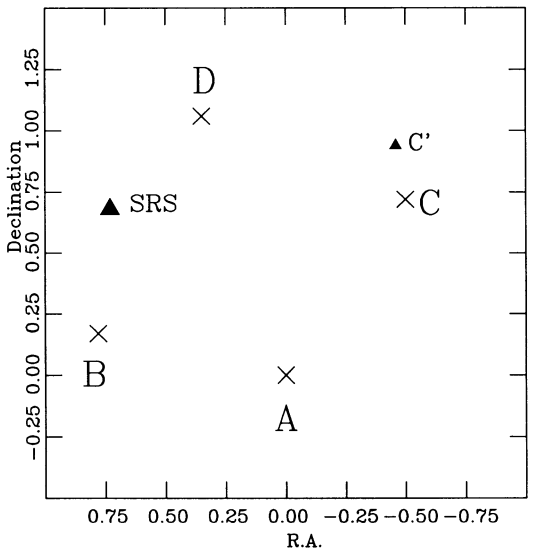

FIG. 3.—Positions of the optical and the radio sources. The positions of the optical and radio images are marked with crosses; the positions of the additional radio sources are marked with triangles (see text).

D coincide quite nicely between each other but that the optical image C is not very well matched in position by its relatively stronger radio counterpart C′ (see the small triangle in Fig. 3) In addition, it seems that a weak extended radio source (WERS) connects the two radio images A and B. In the remainder, we show how a quantitative modeling of the Cloverleaf images may account for most of the above described features.

III. GRAVITATIONAL LENS MODELS

a) Method

An advanced software package, named *GRAL*, for the modeling of gravitational lenses has been developed (by R. K.) over the past few years.

Within the usual limits (weak gravitational fields, small deflection angles), gravitational lensing can be described as a mapping from the image plane (θ_x, θ_y) to the source plane (θ'_x, θ'_y) or, alternatively, from the deflector plane (x, y) to the source plane (ζ, η) by the lens equation

$$\boldsymbol{\theta}' = \boldsymbol{\theta} + \frac{D_{ds}}{D_s}\,\boldsymbol{\alpha}(\boldsymbol{\theta}) \tag{1}$$

$$\boldsymbol{\zeta} = \frac{D_s}{D_d}\,\mathbf{z} + D_{ds}\boldsymbol{\alpha}\,, \tag{2}$$

where $\boldsymbol{\theta}' = (\theta'_x, \theta'_y)$, $\boldsymbol{\theta} = (\theta_x, \theta_y)$, $\boldsymbol{\zeta} = (\xi, \eta)$, $\mathbf{z} = (x, y)$, $\boldsymbol{\alpha} = (\alpha_x, \alpha_y)$ is the (two-dimensional) deflection angle and D_d, D_s, and D_{ds} are apparent size distances.

Usually the modeling of gravitational lenses is done by constructing a deflector model, searching for the images produced by this model and comparing the positions of these images to the observed ones. The model parameters are then changed in order to minimize the difference between observed and constructed image positions. This method, however, is pretty costly, since the images have to be found for each set of model parameters, which consumes a large amount of CPU time, even if the SDF method (Schramm and Kayser 1987) is used. *GRAL* therefore uses a different approach (Kayser 1990).

Obviously for each image i, found at $\boldsymbol{\theta}_i$, of one and the same source s the lens equation must lead to the same result:

$$\boldsymbol{\theta}'_s = \boldsymbol{\theta}'(\boldsymbol{\theta}_i) = \boldsymbol{\theta}'(\boldsymbol{\theta}_j) \quad \forall i, j\,. \tag{3}$$

Thus we simply trace *one* light ray back at each image position and compare the resulting source positions by computing the squared deviation

$$\Delta^2 = \sum_{i \neq j} |\,\boldsymbol{\theta}'(\boldsymbol{\theta}_i) - \boldsymbol{\theta}'(\boldsymbol{\theta}_j)\,|^2\,. \tag{4}$$

We then vary the model parameters (using a numerical evolution process) in order to minimize Δ.

Some care has to be taken to choose appropriate initial values for the procedure, since the model parameter space may well have more than one local minimum of Δ. By applying additional conditions, like limitations on the lens position(s) or the exclusion of the creation of additional bright images, certain parts of the parameter space can be excluded.

In contrast to other authors we make no attempt to fit the brightness ratios of the images. The brightness of the images is subject to intrinsic and microlensing-induced variability as well as to extinction effects; thus values obtained at one epoch are useless for modeling. If eventually the time delay between the images is determined, and microlensing can be separated from intrinsic variability, the true brightness ratios may enter model calculations as parameters.

TABLE 3

RELATIVE IMAGE POSITIONS USED FOR THE MODELS

Image	$\Delta\alpha$	$\Delta\delta$
A	0.″00	0.″00
B	0.78	0.17
C	−0.50	0.72
D	0.35	1.06
SRS.....	0.73	0.68

If a sufficient model has been found, the image configuration is constructed by means of the SDF method (Schramm and Kayser 1987; see also Kayser and Schramm 1988). We then calculate the time delays and the local lensing parameters (convergence, shear, amplification) for the images.

For our models we have used the positions listed in Table 3, which are mainly based on our *B* observations in order to keep as small as possible errors due to reddening caused by an intervening galaxy. We have used a redshift of 1.44 for the deflector, which is a somewhat arbitrary choice given the set of observed absorption systems. However, our aim is mainly to show that the Cloverleaf *can* be produced by simple gravitational lenses, and this conclusion does not depend on the adopted redshift.

We have used $H_0 = 75$ km s^{-1} Mpc^{-1} throughout this paper, as well as a standard Friedmann cosmology with $\Lambda = 0$ and $q_0 = \frac{1}{2}$.

b) Models for the Optical Cloverleaf

Two different models have been used to fit the positions of the four optical images: (*a*) a single elliptical singular isothermal galaxy and (*b*) two spherical singular isothermal galaxies with equal masses. The projected surface density Σ for singular isothermal galaxies is

$$\Sigma = \Sigma_0\, x^{-1}\,, \tag{5}$$

where x is either the radius r (for spherical galaxies) or the major half axis a (for elliptical galaxies).

The one-dimensional central velocity dispersion σ_v is then given by

$$\sigma_v^2 = 2G\Sigma_0\,, \tag{6}$$

where G is the gravitational constant. As discussed by Kent and Falco (1988), flattening reduces σ_v^2 by a factor of $[(1 - e_0^2)^{1/2} \arcsin e_0]/e_0$, where e_0 is the true (edge-on) eccentricity. Since only the eccentricity of the projected surface density is used in the lens models, we can only set an upper limit on σ_v.

The elliptical galaxies have been computed using the algorithm of Schramm (1988, 1990), which is much easier to use than the somewhat cumbersome algorithm of Bourassa and Kantowski (1975).

We have six observables to fit (i.e., three independent relative image positions), and in both models five free parameters to adjust. Thus the models are overconstrained: we find no exact solutions (with zero residual) but one pronounced minimum of the residual with acceptable errors in the image positions.

The results of the simulations are presented in Tables 4 and 5 (model parameters for the best fits; note that *all* parameters have been adjusted simultaneously and none has been fixed during the modeling process), and in Figures 4 and 5 (image and source plane plots, including critical curves and caustics).

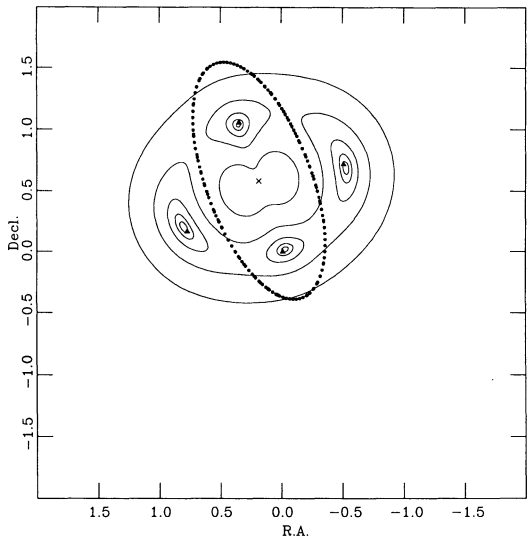

FIG. 4a

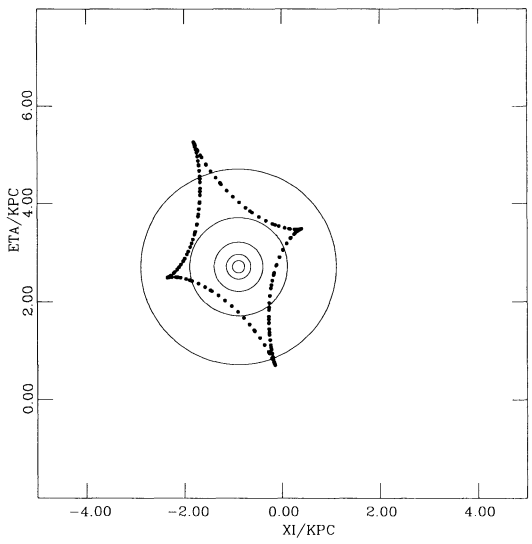

FIG. 4b

FIG. 4.—Model 1 (*a*) images and critical curves, (*b*) source and caustics. The source radii are 125, 250, 500, 1000, and 2000 pc, respectively. The galaxy centers are marked with crosses; the black triangles correspond to the observed image positions. The dotted lines are the critical curves and caustics, respectively.

TABLE 4

PARAMETERS OF MODEL 1

Parameter	Value
Galaxy type	Elliptical singular isothermal
Surface density	$\Sigma(a) = \Sigma_0 a^{-1}$
Position	(−0.″19, 0.″58)
Eccentricity	0.903
Position angle	70°
Density parameter Σ_0	$1.77 \times 10^7\ M_\odot\ \mathrm{pc}^{-1}$
Velocity dispersion σ_v	$<285\ \mathrm{km\ s}^{-1}$

As can be seen from the figures, both models fit equally well the optical Cloverleaf observations. Model 2, however, produces an additional weak image between the centers of the two galaxies.

These models are best fits for the observed image positions as given in Table 3. Errors in the resulting model parameters due to errors in these image positions have been estimated by varying the image positions. An error in the image positions of 0.″01 (0.″1) leads to errors of the order of 0.″004 (0.″08) in the

TABLE 5

PARAMETERS OF MODEL 2

Parameter	Value
Galaxy type	Spherical singular isothermal
Surface density	$\Sigma(r) = \Sigma_0 r^{-1}$
Galaxy 1 position	(−0.″53, 0.″34)
Galaxy 2 position	(0.″21, 0.″65)
Density parameter Σ_0	$6.05 \times 10^6\ M_\odot\ \mathrm{pc}^{-1}$
Velocity dispersion σ_v	$228\ \mathrm{km\ s}^{-1}$

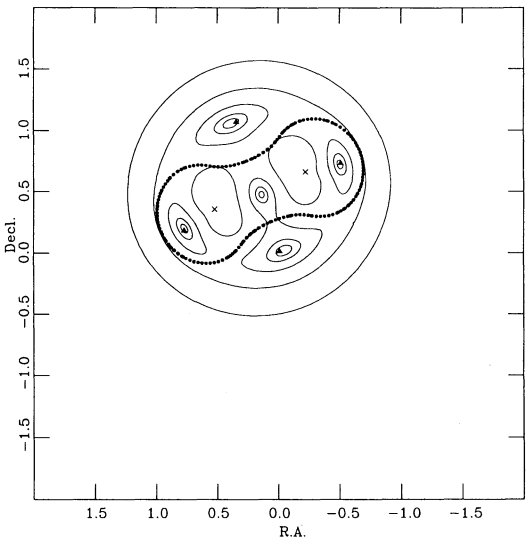

FIG. 5a

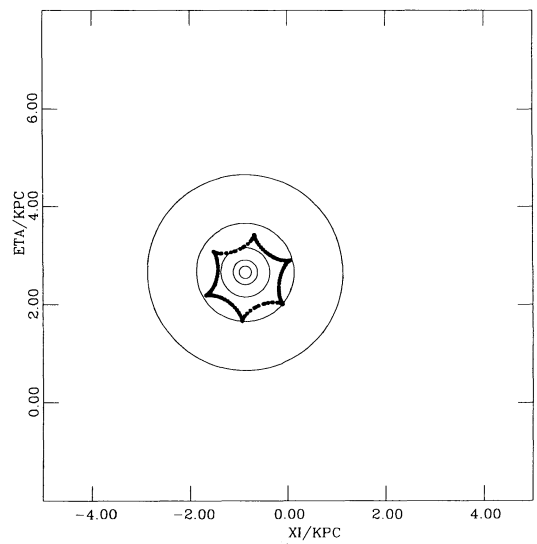

FIG. 5b

FIG. 5.—Model 2 (*a*) images and critical curves, (*b*) source and caustics.

TABLE 6

TIME DELAYS

Images	Model 1	Model 2
A – B.....	$-24^d.9$	$19^h.2$
B – C.....	3.0	1.8
C – D.....	42.6	−30.7
D – A.....	−20.6	9.6

TABLE 8

PREDICTED MICROLENSING AMPLIFICATIONS

Image	Model 1	Model 2
A.....	2.08	1.44
B.....	1.01	2.57
C.....	1.00	3.23
D.....	2.11	1.00

x-position and 0".01 (0".1) in the y-position of the deflector galaxy, 4×10^3 (3×10^4) $M_\odot$ pc^{-1} in the density parameter Σ_0. 0.004 (0.4) in the eccentricity and 1° (20°) in the position angle. These results should, however, not be overinterpreted: our calculations are just examples to demonstrate that plausible models are possible for this object.

In Table 6, we present the expected time delays between the images in our models. Due to the symmetry of the configuration, the time delays are fairly small; it thus should be possible to measure them within one observing season (if H1413+117 shows sufficient intrinsic variability). As can be seen, the time delays are strongly model-dependent; thus the time delays, if eventually determined, can be used to rule out certain models.

From the macromodels we can calculate the *local* lensing parameters (compare Kayser 1990) at each image i.e., the convergence κ and the shear γ', as well as the amplification

$$A_G = |(1 - \kappa - \gamma')(1 - \kappa + \gamma')|^{-1} \quad (7)$$

for the smooth deflector (Table 7). The parameters κ and γ' are important for the prediction of microlensing effects. Note that κ equals the total surface mass density σ_t in units of the critical density

$$\sigma_{\rm crit} = \frac{1}{\pi} \frac{c^2}{4G} \frac{D_s}{D_{ds} D_s}, \quad (8)$$

which would lead to a complete focusing of a bundle of light rays (in the absence of shear). For H1413+117 the critical density is $\sigma_{\rm crit} = 6050\, M_\odot$ pc^{-2}.

In both models, the brightness ratios of the images turn out to be quite different from the observed ones. This may, however, be explained by intrinsic variability and/or microlensing.

If we assume that H1413+117 shows *no* intrinsic variability, we can compare the observed brightness ratios with the ones predicted by our models under the assumption that the differences are due to microlensing. In Table 8, we list the predicted microlensing amplifications computed under these assumptions. We have here used the *B* magnitudes, since they are less subject to reddening than the *I* or *R* magnitudes. Note that the microlensing amplifications can only be predicted up to a constant factor, since the true source luminosity is not known. We have normalized the amplification such that the minimum amplification is 1.

TABLE 7

LOCAL LENSING PARAMETERS

	κ		$\lvert\gamma'\rvert$		AMPLIFICATION	
IMAGE	Model 1	Model 2	Model 1	Model 2	Model 1	Model 2
A.....	0.83	0.52	0.83	0.14	1.5	4.9
B.....	0.31	0.73	0.30	0.72	2.6	2.3
C.....	0.31	0.79	0.30	0.78	2.6	1.8
D.....	1.05	0.49	1.04	0.18	0.9	4.3
E.....	...	0.87	...	0.86	...	1.4

Interestingly, in model 1 two of the four images, B and C, do not need any microlensing influence. In this model, image D is expected to show the largest microlensing amplification. The observed fading of image D within the 19 days between our observations, may thus correspond to the second part of a high amplification event due to the crossing of a microcaustic (Kayser, Refsdal, and Stabell 1986; Grieger, Kayser, and Refsdal 1988).

For each macroimage, the possible microlensing parameters σ (normalized number densities of microlenses) and γ (normalized shear), as introduced by Paczyński (1986) and Kayser, Refsdal, and Stabell (1986), lie on the straight line

$$\sigma = 1 + \frac{\sigma_t - 1}{\gamma'} \gamma \quad (9)$$

in the σ-γ plane; compare Kayser and Refsdal (1989) and Kayser (1990), where σ_t is the total (projected) surface density, in units of the critical density $\sigma_{\rm crit}$, (see eq. [8]). Since the sign of γ' and γ, respectively, depends on the chosen coordinate system, we can restrict ourselves to $\gamma \geq 0$ without loss of generality. Note that sign (γ) = sign (γ') for $\sigma_c < 1$, and sign (γ) = −sign (γ') for $\sigma_c > 1$ ("overfocusing"), where σ_c is the surface density of the homogeneously distributed matter in units of $\sigma_{\rm crit}$.

Since the fraction ϵ of matter contained in stars is obviously limited by $0 \leq \epsilon \leq 1$, we find that (*a*) for $\sigma_t < 1$, only scenarios with $0 < \sigma < \sigma_t$ are allowed, and (*b*) for $\sigma_t > 1$, only scenarios with either $\sigma > \sigma_t$ or $\sigma < 0$ (overfocusing) are allowed. In Figure 6, we show the allowed parameter combinations (σ, γ) for the images of H1413+117 in our models. Again, image D in model 1 is expected to show the strongest influence due to microlensing.

c) *The Strong Radio Source*

From our models we see that SRS lies right on the critical curve of the deflector. This is a very generic feature, since every possible lens model for H1413+117 *must* lead to a critical curve between each two of the images. Thus, SRS can be explained by an additional radio feature, e.g., an ejected blob, of the quasar, located on the lens caustic and thereby being strongly amplified. We have tried to reproduce the radio contour map by adding a second circular source to the quasar core. The location of this source is found by tracing SRS back to the source plane in the used model. The linear separation between the QSO and SRS is 1085 pc (corresponding to 0".21) in model 1 and 780 pc (0".15) in model 2, respectively.

Figures 7 and 8 show the results of these simulations. In both models, SRS can be reproduced nicely. Additional images are created near A and C in both models. The additional radio image near C may possibly explain the observed misplacement of C′ relatively to C.

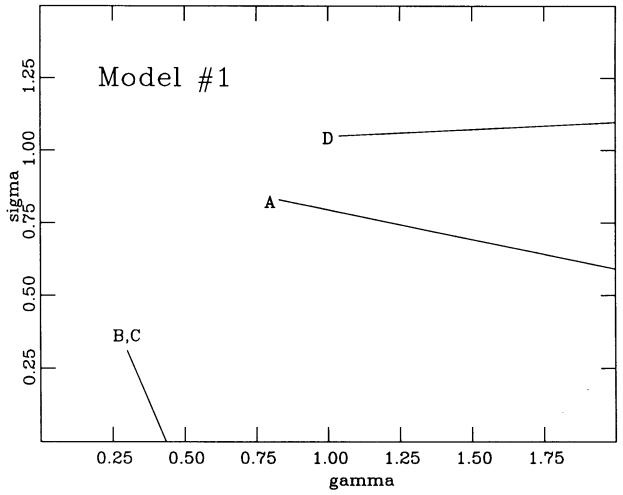

FIG. 6*a*

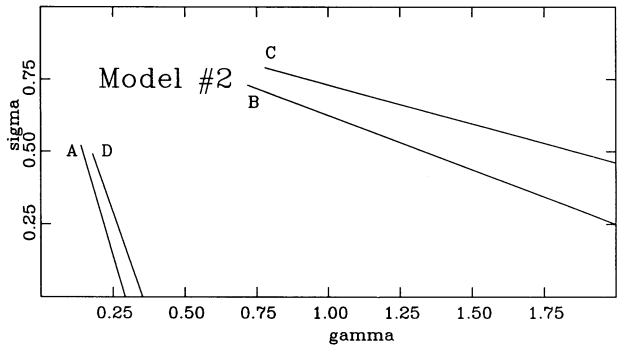

FIG. 6*b*

FIG. 6.—Allowed microlensing parameters for the images in (*a*) model 1 and (*b*) model 2

In model 1, the second additional radio image lies right between A and B, thereby offering an explanation for WERS. Since WERS, like SRS, lays near or on the critical curve, another possibility to explain WERS is a jet crossing the caustic of the lens, thereby becoming strongly amplified only in a small region. The quality of our present data is, however, not sufficient to allow for a more detailed modeling of the extended structure of the radio source.

IV. DISCUSSION AND OUTLOOK

Both of our adopted models fit remarkably well the optical Cloverleaf observations, as well as the radio structure of H1413+117 including SRS, thereby supporting the hypothesis that H1413+117 is indeed a gravitationally lensed quasar.

However, since both models are quite different, our simulations show also that at this stage, we are far from obtaining one unique model for the object. More and better observational data are needed in order to produce a larger set of parameters to be fitted, thereby reducing the allowed range of parameter space.

Especially, a better VLA map would be very useful, since this would offer the possibility of a more accurate modeling of the extended radio source by means of the combined DiSI/DiSoR method proposed by Kayser and Schramm (1988). Note that a very similar method has later been used by Kochanek *et al.* (1989) for the successful modeling of the Einstein Ring MG 1131+0456.

Monitoring of the Cloverleaf should also have high priority, since the time delays are very sensitive to the model. Besides, the measurement of the time delays is the only *real* proof of the lens scenario (see Narasimha and Narlikar 1989 for an alternative explanation of multiple quasars).

The time delays predicted from our models are sufficiently short to allow a determination within one observational season, making H1413+117 an exceptionally well suited object for gravitational lens research. Microlensing may, however, make it difficult to separate the intrinsic variability from the observed light curves. On the other hand, since the expected time delays are short, it should be easy to prove whether observed variability is due to microlensing or not.

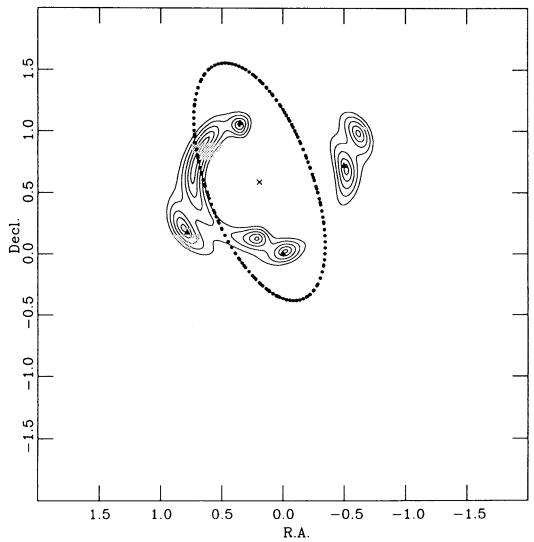

FIG. 7.—Model 1: Quasar and SRS. Images produced by two circular sources of equal brightness: (*a*) the quasar (position defined by back-tracing the quasar images) and (*b*) a radio blob (position defined by back-tracing SRS).

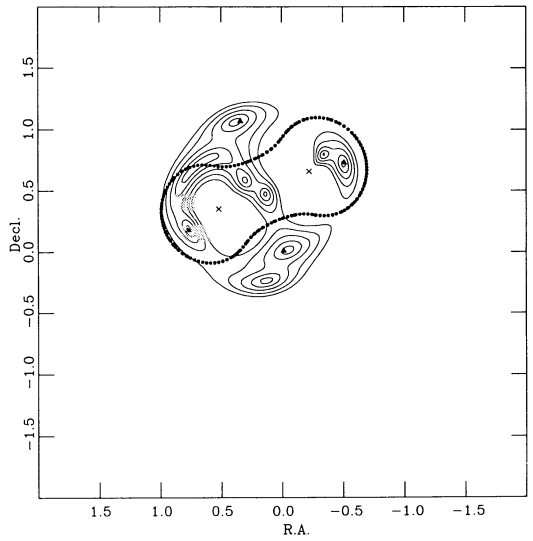

FIG. 8.—Model 2: Quasar and SRS

It is a pleasure to thank Thomas Schramm (Hamburg) for the implementation of the elliptical deflector code into the *GRAL* package. R. K. acknowledges support by a NATO research scholarship, granted by the German Academic Exchange Service (DAAD). J. S. acknowledges partial support during this research from NATO grant No. 0161/87. A. S. thanks Eric Gosset and the Φ.V. for a lot of support. The National Radio Astronomy Observatory is operated by Associated Universities, Inc., under a cooperative agreement with the US National Science Foundation.

REFERENCES

Blandford, R., and Kochanek, C. 1987, in *Dark Matter in the Universe*, ed. J. Bahcall *et al.* (Singapore: World Scientific), p. 133.
Borgeest, U. 1986, *Ap. J.*, **309**, 467.
Bourassa, R. R., and Kantowski, R. 1975, *Ap. J.*, **195**, 13.
Canizares, C. R. 1981, *Nature*, **291**, 620.
———. 1982, *Ap. J.*, **263**, 508.
Crampton, D., McClure, R. D., Fletcher, J. M., and Hutchings, J. B. 1989, *A.J.*, **98**, 1188.
Drew, J. E., and Boksenberg, A. 1984, *M.N.R.A.S.*, **211**, 813.
Gorenstein, M. V., Falco, E. E., and Shapiro, I. I. 1988, *Ap. J.*, **327**, 693.
Gott, J. R., III. 1981, *Ap. J.*, **243**, 140.
Grieger, B., Kayser, R., and Refsdal, S. 1988, *Astr. Ap.*, **194**, 54.
Hazard, C., Morton, D. C., Terlevich, R., and McMahon, R. 1984, *Ap. J.*, **282**, 33.
Hewitt, J. N. 1989, *Cosmic Strings: the Current Status*, ed. L. Kraus and F. S. Accetta, in press.
Hewitt, J. N., Burke, B. F., Turner, E. L., Schneider, D. P., Lawrence, C. R., Langston, G. I., and Brody, J. P. 1989, in *Gravitational Lenses*, ed. J. M. Moran *et al.* (New York: Springer-Verlag), p. 147.
Kayser, R. 1986, *Astr. Ap.*, **157**, 204.
———. 1990, *Ap. J.*, **357**, 309.
Kayser, R., and Refsdal, S. 1983, *Astr. Ap.*, **128**, 156.
———. 1989, *Nature*, **338**, 745.
Kayser, R., Refsdal, S., and Stabell, R. 1986, *Astr. Ap.*, **166**, 36.
Kayser, R., and Schramm, T. 1988, *Astr. Ap.*, **191**, 39.
Kent, S. M., and Falco, E. E. 1988, *A.J.*, **96**, 1570.
Kochanek, C. S., Blandford, R. D., Lawrence, C. R., and Narayan, R. 1989, *M.N.R.A.S.*, **238**, 43.
Magain, P., Surdej, J., Swings, J.-P., Borgeest, U., Kayser, R., Kühr, H., Refsdal, S., and Remy, M. 1988, *Nature*, **334**, 325.
Narasimha, D., and Narlikar, J. V. 1989, *Ap. J.*, **338**, 44.
Nottale, L. 1988, *Ann. de Phys.*, **13**, 223.
Paczyński, B. 1986, *Ap. J.*, **301**, 503.
Refsdal, S. 1964, *M.N.R.A.S.*, **128**, 307.
Refsdal, S., and Kayser, R. 1989, in *The Post-Recombination Universe* (NATO-ASI Series C), **240**, 297.
Schneider, P. 1988, *Astr. Ap.*, submitted.
Schramm, T. 1988, Ph.D. thesis, University of Hamburg.
———. 1990, *Astr. Ap.*, **231**, 19.
Schramm, T., and Kayser, R. 1987, *Astr. Ap.*, **174**, 361.
Surdej, J. 1990, in *Gravitational Lenses*, ed. Y. Mellier, B. Fort, and G. Soucail (Berlin: Springer-Verlag), p. 57.
Surdej, J., *et al.* 1987, *Nature*, **329**, 695.
Surdej, J., *et al.* 1988*a*, *Astr. Ap.*, **198**, 49.
Surdej, J., *et al.* 1988*b*, *Proc. of Workshop on Optical Surveys for Quasars* (*A.S.P. Conf. Ser.*, **2**), p. 183.
Turner, E. L. 1988, in *Dark Matter*, ed. J. Audouze and Tran Thanh Van.
———. 1989, *Proc. 14th Texas Symp., Relativistic Astrophysics*, in press.
Turner, E. L., Ostriker, J. P., and Gott J. R., III. 1984, *Ap. J.*, **284**, 1.
Turnshek, D. A., Foltz, C. B., Grillmair, C. J., and Weymann, R. J. 1988, *Ap. J.*, **325**, 651.
Walsh, D., Carswell, R. F., and Weymann, R. J. 1979, *Nature*, **279**, 381.
Webster, R. L., Hewett, P. C., Harding, M. E., and Wegner, G. A. 1988, *Nature*, **336**, 358.
Webster, R. L., Hewett, P. C., and Irwin, M. J. 1988, *A.J.*, **95**, 19.
Zwicky, F. 1937*a*, *Phys. Rev.*, **51**, 290.
———. 1937*b*, *Phys. Rev.*, **51**, 679.

JAMES J. CONDON: National Radio Astronomy Observatory, Edgemont Road, Charlottesville, VA 22903
[E-mail: jcondon@nrao.edu]

RAINER KAYSER: Hamburger Sternwarte, Gojenbergsweg 112, D-2050 Hamburg 80, Federal Republic of Germany
[E-mail: st40010@dhhuni4.bitnet]

KENNETH I. KELLERMANN: National Radio Astronomy Observatory, Edgemont Road, Charlottesville, VA 22903
[E-mail: kkellerm@nrao.edu]

PIERRE MAGAIN: Institut d'Astrophysique, Université de Liege, Avenue de Cointe 5, B-4200 Cointe-Ougrée, Belgium
[E-mail: u2182pm@bliulg11.bitnet]

MARC REMY: European Southern Observatory, La Silla, Casilla 19001, Santiago 19, Chile
[E-mail: remy@dgaeso51.bitnet]

ALAIN SMETTE: European Southern Observatory, Karl-Schwarzschild-Straße 2, D-8046 Garching bei München, Federal Republic of Germany
[E-mail: smette@dgaeso51.bitnet]

JEAN SURDEJ: Institut d'Astrophysique, Université de Liege, Avenue de Cointe 5, B-4200 Cointe-Ougrée, Belgium
[E-mail: u2141js@bliulg11.bitnet]